ornl

ORNL/TM-11176

OAK RIDGE
NATIONAL
LABORATORY

MARTIN MARIETTA

Sulfidation/Oxidation Properties of Iron-Based Alloys Containing Niobium and Aluminum

J. H. DeVan
H. S. Hsu
M. Howell

Fossil
Energy
Program

OPERATED BY
MARTIN MARIETTA ENERGY SYSTEMS, INC.
FOR THE UNITED STATES
DEPARTMENT OF ENERGY

ORNL/TM--11176

DE89 013766

Metals and Ceramics Division

SULFIDATION/OXIDATION PROPERTIES OF IRON-BASED ALLOYS CONTAINING NIOBIUM AND ALUMINUM

J. H. DeVan
H. S. Hsu
M. Howell

Date Published: May 1989

Notice: This document contains information of a preliminary nature. It is subject to revision or correction and therefore does not represent a final report.

Research sponsored by the
U.S. Department of Energy,
Advanced Research and Technology Development
Fossil Energy Materials Program
(AA 15 10 10 0)

Prepared by the
OAK RIDGE NATIONAL LABORATORY
Oak Ridge, Tennessee 37831-6285
operated by
MARTIN MARIETTA ENERGY SYSTEMS, INC.
for the
U.S. DEPARTMENT OF ENERGY
under contract DE-AC05-840R21400

CONTENTS

LIST OF TABLES

LIST OF FIGURES

SULFIDATION/OXIDATION PROPERTIES OF IRON-BASED ALLOYS CONTAINING NIOBIUM AND ALUMINUM*

J. H. DeVan, H. S. Hsu, and M. Howell

ABSTRACT

Compatibility with mixed gases containing S, O, and Cl is a critical requirement for high-temperature alloys used in coal conversion and combustion applications. Comparative corrosion tests of Fe-25Cr-20Ni, Fe-18Cr-6Al, and Fe-9Cr-9Nb-6Al (wt %) at 700 to 800°C in a simulated coal gasification environment led to the development of Fe-Nb-Al alloys and testing of both Fe-Nb-Al and Fe_3Al alloys. The niobium and aluminum content in the latter alloys ranged from 8 to 18 and 6 to 16 wt %, respectively. The niobium addition was intended as a selective refractory sulfide former. Testing was carried out at 700 to 800°C in H_2S-H_2-H_2O gas mixtures with relatively low oxygen activities ($\leq 10^{-22}$ atm) and high sulfur activities ($\geq 10^{-6}$ atm).

Metallographic and chemical analyses of the corrosion product scales and the underlying alloy were performed to determine the role of the respective metallic elements on sulfidation/oxidation processes. Results showed that adding niobium led to the growth of niobium sulfides in association with discrete Fe_2Nb particulates in the alloys but not with the matrix phase, which was much lower in niobium content. The matrix phase was extremely resistant to sulfidation in alloys containing 12% Al and behaved similarly to a Fe-15.8Al alloy. A major finding in these studies was the complete suppression of iron-sulfide formation by aluminum at concentrations of 12% and above.

INTRODUCTION

One of the critical issues in technologies that use coal directly as a fuel or that convert it to other fuel forms, such as liquids or gases, is the compatibility of structural materials with the environment. Because of mineral ash, sulfur, chlorine, and other impurities in coal, the metallic components in coal utilization and conversion systems are

---

*Research sponsored by the U.S. Department of Energy, AR&TD Fossil Energy Materials Program [DOE/FE AA 15 10 10 0, Work Breakdown Structure Element ORNL-3(A)] under contract DE-AC05-84OR21400 with Martin Marietta Energy Systems, Inc.

subject to severe corrosion. These components include gas coolers in gasification systems; superheaters and reheaters in pulverized-coal boilers and industrial coal-fired boilers; and heat exchangers in fluidized-bed combustors, hot gas cleanup systems, and direct coal-fired heat engines. Both ferritic and austenitic iron-based alloys are frequently used in these coal-related applications.

Most of the alloys or metallic coatings that are designed to withstand high-temperature degradation in aggressive environments rely on the formation of protective Cr_2O_3 or Al_2O_3 scales. In general, such alloys possess good resistance to high-temperature oxidation. However, when operating in mixed-oxidant environments, such as those found in coal utilization and conversion processes (which contain O, S, and Cl), protective oxide scales may either not form or eventually break down, thus allowing rapid corrosion of the base alloy. Extensive corrosion studies have been conducted over the past few decades to characterize the corrosion behavior of heat-resistant alloys in coal-derived environments and to define the role of alloying elements in the corrosion processes.[1] This study has a similar objective: namely, to establish the effectiveness of aluminum and niobium in conferring corrosion resistance to iron-based alloys for sulfidizing/oxidizing environments. The corrosion environment used for this evaluation ($H_2S + H_2 + H_2O$) is representative of coal gasification processes, and the temperature range selected for study (700–800°C) is of interest for the economizer heat exchangers being developed for cooling the gasifier product gas.

As a first step in developing more corrosion-resistant alloys for coal-derived environments, we compared the corrosion behavior of Fe-25Cr-20Ni* and Fe-18Cr-6Al in a H_2S-H_2-H_2O-Ar gas mixture at 800°C ($P_{S_2} = 10^{-6}$ atm, $P_{O_2} = 10^{-20}$ atm) (ref. 2). The Fe-Cr-Ni alloy corroded rapidly under the test conditions, the corrosion products containing principally iron and chromium sulfides. Corrosion rates for the Fe-Cr-Al alloy were significantly lower and were reduced still further by preoxidation treatments at 800°C before exposure to the mixed gas. However, examination of the corrosion product showed that although a

*All alloy compositions are in weight percent.

stable Al_2O_3 film formed and remained on the alloy surface, it became overgrown by thick platelets of an iron-rich sulfide, $(Fe_{0.73}Cr_{0.24}Al_{0.03})S$. Preoxidation significantly reduced the extent of sulfidation in 100-h tests, but sulfide platelets nevertheless developed at isolated locations on the surface, apparently associated with mechanical defects in the oxide. These tests proved the chemical stability of Al_2O_3 under the test conditions. However, they also showed the need for improving the mechanical stability of the oxide as a corrosion product layer and for suppressing the formation of sulfide compounds once the oxide is breached. The approach adopted was to increase the Al concentration of the alloy, to eliminate Cr as an alloying addition, and to add a refractory sulfide former, *viz*, Nb.

RATIONALE FOR NIOBIUM AND ALUMINUM AS ALLOYING ADDITIONS

Alloys that rely on the formation of Cr_2O_3 scales for protection in high-temperature oxygen-containing environments are prone to sulfide formation in mixed gases with relatively high sulfur partial pressures and low oxygen partial pressures.[1,2] Because of their potential for forming low-melting metal-metal sulfide eutectics, nickel- and/or cobalt-containing alloys are also unsuitable for high-temperature mixed gases with high P_{S_2} and low P_{O_2}. Because the equilibrium oxygen partial pressure at the Al_2O_3/Al_2S_3 phase boundary is seven orders of magnitude lower than that of Cr_2O_3/Cr_XS_y at a given sulfur activity, Al_2O_3 is thermodynamically stable in most coal-related environments. (Cr_XS_y is used here to designate chromium sulfides with different stoichiometries.) Thus, Al_2O_3-forming iron-based alloys have tended to be more corrosion resistant than Cr_2O_3-forming iron-based alloys in mixed gases containing sulfur.[1,2]

In mixed gases, sulfidation of conventional Al_2O_3-forming alloys of the type Fe-Cr-Al, with and without preoxidation, proceeds initially with the nucleation and growth of chromium-rich sulfides at certain sites in the alumina scale and later with the formation of iron-rich sulfides.[2] These reactions appear to be associated with both the diffusion of sulfur through the oxide scale and the mechanical cracking of the scale. To overcome these effects, alloy modifications are needed to enhance the

rapid reformation of Al_2O_3 and to eliminate the chemical effects of sulfur diffusion in the scale, as manifested by sulfide formation under the oxide scale. An obvious approach for meeting the former requirement is to increase the aluminum concentration in the alloy and facilitate the supply of aluminum to the corroding surface. A complementary approach that addresses both requirements is to add a sulfide-forming metal that, in contrast to chromium, forms a more passive, slow-growing sulfide corrosion product. According to the review by Mrowec and Przybylski,[3] refractory metal sulfides, such as NbS_2, MoS_2, and WS_2, are characterized by uniquely low self-diffusion coefficients. This fact is attested by the sulfidation rate of niobium at 800°C, which is some seven orders of magnitude lower than that of iron. Strafford and Bird[4] also report that the corrosion rate of Nb in 25% H_2S-75% H_2 at 800°C was about the same order of magnitude as the oxidation rate of Cr in pure O. It is therefore of interest to establish whether conditions exist in a mixed-gas (H-S-O) environment under which adding niobium to an iron-aluminum alloy will lead to the formation of a niobium-sulfide barrier layer that would facilitate the protectiveness of the dominant Al_2O_3 oxidation product.

EXPERIMENTAL

The compositions of the alloys used in this study are listed in Table 1. The alloys were prepared by arc-melting high-purity component metals under argon and drop-casting into a 25.4-mm-diam by 127-mm-long mold. The ingots were homogenized by annealing under argon for 4 h at 1200°C. They were then hot swaged at 1120°C to 12.7-mm-diam bars, annealed for 20 min at 1120°C, air cooled, and descaled. Specimens in the form of 0.66- by 12.7-mm-diam disks were cut perpendicular to the bar axis using a diamond slitting saw, and the two circular faces of the specimens were mechanically abraded using 320-grit followed by 600-grit SiC abrasive paper. In the case of one of the alloys (PS10 in Table 1), the arc-cast ingot was clad with stainless steel, heated for 2 h at 1200°C, and immediately hot extruded to 10.7-mm diam. Specimens of this diameter were prepared using the same thickness and surface preparation as described previously.

Table 1. Nominal compositions of test alloys

Alloy designation	Concentration (wt %)			
	Al	Nb	Cr	Fe
PS2	6		18	76
PS3	6	9	9	76
PS4	6	18		76
PS8	12	18		70
PS10[a]	12	18		70
PS15	12	12		76
PS14	12	8		80
PS11	15.8			84.2

[a]Hot extruded.

During exposure to the mixed-gas environment, the weight changes of the specimens were continuously recorded using an Ainsworth microbalance. Each specimen was suspended in a quartz reaction tube and heated by an external tubular resistance furnace. Test temperatures ranged from 700 to 800°C and exposure times from 20 to 193 h. To prevent separation of the component gas species caused by thermal diffusion, the gas mixture was preheated and flowed upward within the reaction tube at a flow rate of ~1.67 cm^3/s. Platinum foil was located inside the hot zone of the reaction tube to enable the gas mixture to reach its equilibrium state. To control the sample's position, a magnetic device was used to lower the specimen into the hot zone of the reaction tube, which had been purged with the gas mixture for at least 2 h before the corrosion experiment. A schematic of the test apparatus is shown in Fig. 1.

Gas mixtures used in this study contained hydrogen sulfide and argon that were premixed to the desired compositions by the Matheson Gas Products Company. The compositions of the gas mixtures and their equilibrium pressures of oxygen and sulfur are given in Table 2. Moisture

ORNL-DWG 88-14007

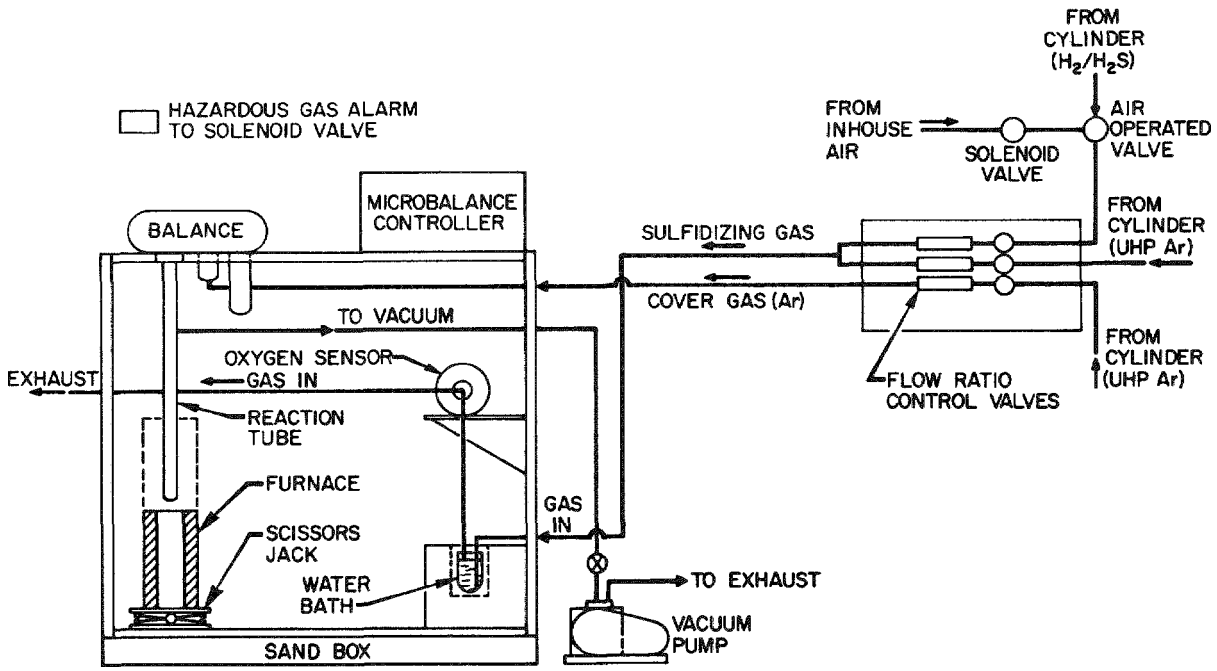

Fig. 1. Test apparatus for sulfidation/oxidation studies.

Table 2. Compositions and S_2/O_2 fugacities of gas mixtures used for corrosion studies

Mixture number	Test temperature (°C)	Gas species (vol %)				log P_{O_2}	log P_{S_2}
		H_2S	H_2	H_2O	Ar		
1	800	0.0548	0.83	1.43	97.68	−17.9	−6.0
2	800	0.55	8.38	1.46	89.61	−19.9	−6.0
3	800	0.95	14.11	2.46	82.48	−19.9	−6.0
4	800	5.35	79.23	1.70	13.72	−21.7	−6.0
5	700	0.184	0.97	0.255	98.59	−22.0	−6.0
6	700	17.61	9.27	2.37	70.75	−22.0	−4.0

was added to the gas mixture by bubbling the gas through a temperature-controlled water bath. The oxygen partial pressure in the gas was continuously monitored by a Y_2O_3-stabilized ZrO_2 oxygen sensor. The equilibrium partial pressure of sulfur at the reaction temperature was calculated from the known composition of the gas mixture using published thermodynamic data. The gas mixture and test temperature were selected to simulate projected sulfur and oxygen activities in gases derived from coal.[5]

The conditions of exposure for the various test specimens are listed in Table 3. As more corrosion-resistant compositions were developed, the time of exposure and the H_2S concentration of the test environment were increased, and the H_2:H_2O ratio was adjusted to lower the partial pressure of oxygen from 10^{-20} to 10^{-22} atm. Accordingly, the later alloys in the test series (PS8, 10, 11, 14, and 15 in Table 1) were exposed to a more aggressive corrosion environment than were the initial alloys. Experiments were begun by lowering a cold specimen into the hot zone of the reaction tube and stopped by quenching the specimen to room temperature in high-purity argon. Both optical and scanning electron microscopes (SEMs) were used to examine the morphology of corrosion scales, whereas energy-dispersive X-ray spectroscopy (EDS) was used to determine the composition of the scales.

RESULTS

Initial tests were conducted to determine the effect of substituting niobium for chromium in alloys containing 6% Al. Figure 2 compares the thermogravimetric results for alloys with all or part of the chromium replaced by niobium (PS3 and PS4) with the Fe-18Cr-6Al alloy (PS2). Note that lowering the chromium level to 9% with 9% niobium added (PS3) reduced the weight gain only slightly compared with PS2. However, replacing all of the chromium with niobium (PS4) significantly reduced the weight gain. Figures 3(*a*) and 3(*b*) show surface topographies of PS2 exposed to H_2S-H_2-H_2O mixture 2 (Table 2) at 800°C for 5 and 10 min, respectively. During the early stage of corrosion, spherical or multifaceted corrosion product nuclei formed on the alloy surface. Semiquantitative EDS analysis

Table 3. Test conditions for thermogravimetric analyses (TGA)

Alloy	Test number	Gas mixture	Temperature (°C)	Total exposure time (h)
PS2	017	2	800	0.167
	018	2	800	0.50
	019	2	800	0.083
	023	2	800	24
	025	2	800	65
	026	2	700	92
	027	2	800	5
	028	2	700	2
PS3	001	2	800	24
	002	2	800	24
	012	4	800	6
PS4	006	1	800	92
	007	1	800	25
	008	2	800	74
	010	2	800	50
	011	3	800	40
PS8	001	2	800	75
	003	3	800	141
	004	5	700	50
	006	6	700	50
	007	4	800	125
PS10	001	3	800	161
	002	6	700	89
	003	4	800	52
PS11	001	4	800	290
	003	4	800/30[a]	305
PS14	001	4	800	168
PS15	001	4	800	171

[a]Thermal cycled to room temperature every 48 h.

indicated that the nuclei were sulfides with the composition $(Cr_{0.48}Fe_{0.3}Al_{0.22})S$, with the total of cations in the sulfide normalized to one. Because of the inability of EDS to detect light elements, the oxygen content of the nuclei is not known. Therefore, the corrosion product formed on PS2 can be either a mixed sulfide (Cr,Fe,Al) or a mixture of (Cr,Fe)S and Al_2O_3.

ORNL-DWG 89-2177

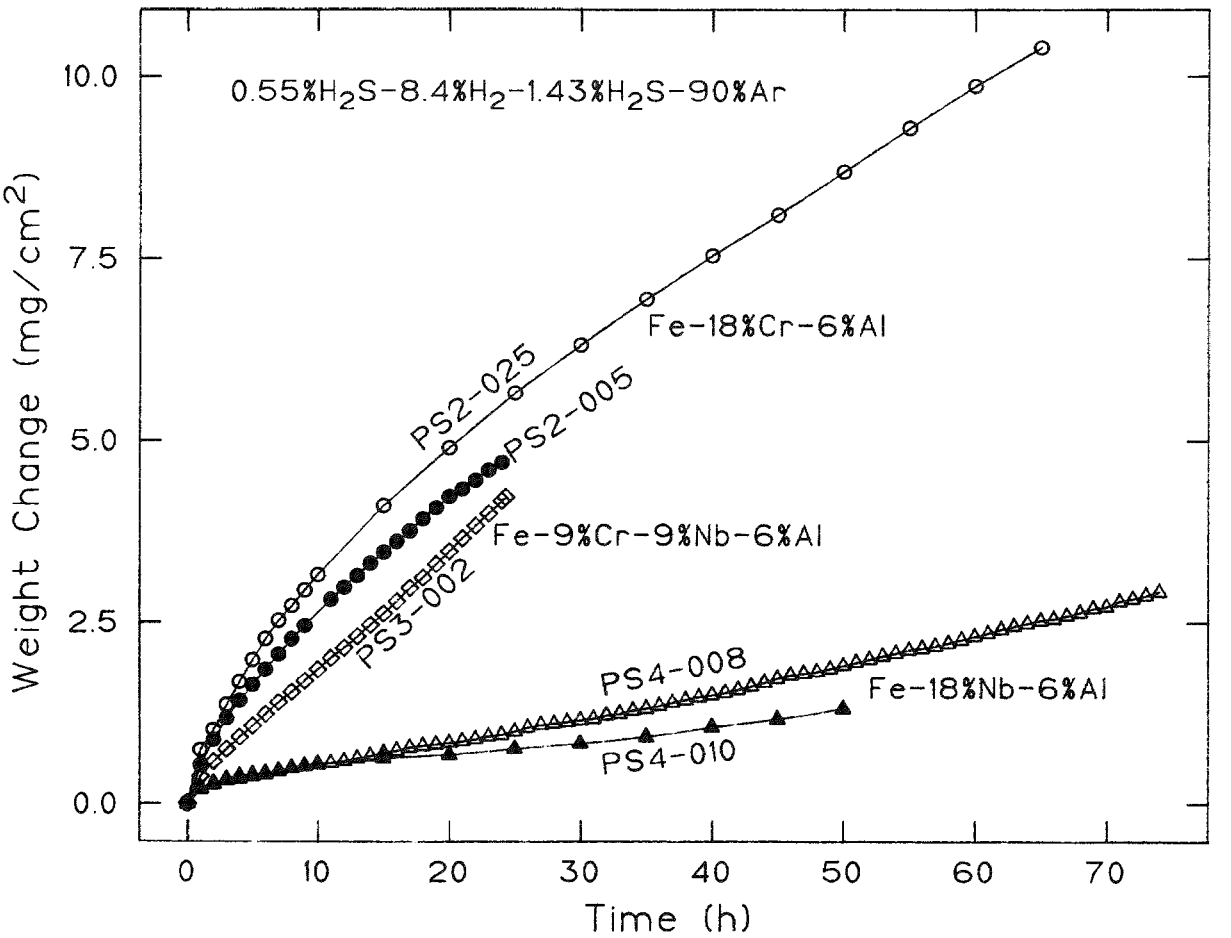

Fig. 2. Effect of replacing chromium with niobium on weight gain of 6% Al alloys at 800°C.

After a 30-min exposure to gas mixture 2 with P_{S_2} = 10^{-6} and P_{O_2} = 10^{-20} atm at 800°C, sulfide platelets began to form, as shown in Fig. 4(*a*). These sulfide platelets, $(Fe_{0.72}Cr_{0.2}Al_{0.08})S$, have a much higher concentration of iron compared with the more spherical sulfides formed during the early stage of exposure. The iron-rich sulfide was also found on some surfaces of the crystalline chromium-rich sulfide. [Note that $(Cr_{0.44}Fe_{0.36}Al_{0.2})S$ is in the upper left of the micrograph in Fig. 4(*b*), but the chromium-rich sulfide grain in the lower right of the micrograph is covered almost entirely with the iron-rich sulfide.] Apparently, the iron-rich sulfide grows more quickly than does the

M25353

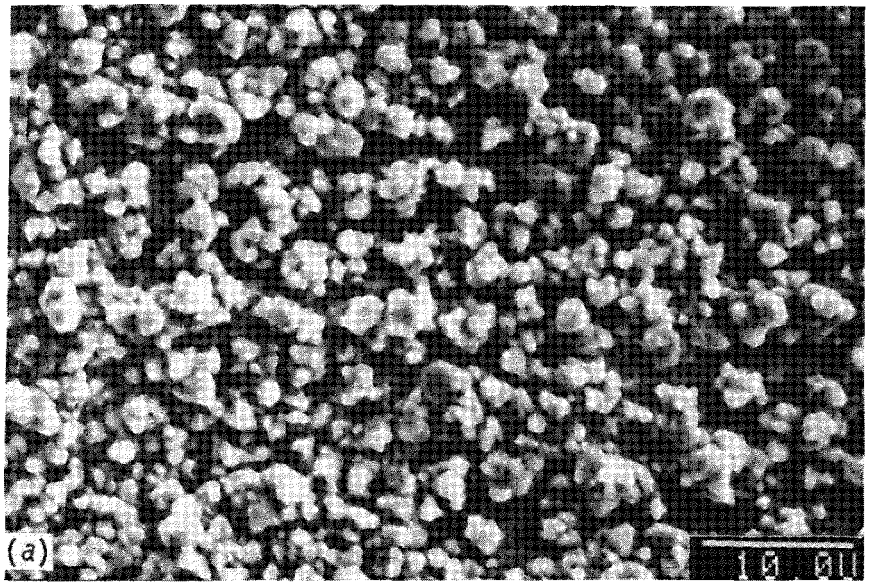

M25401

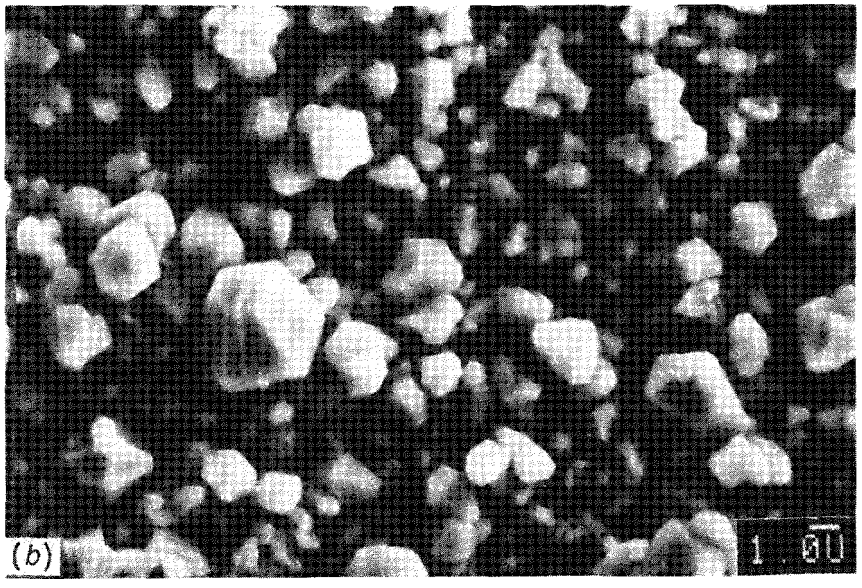

Fig. 3. Surface topographies of PS2 (Fe-18Cr-6Al) exposed to the gas mixture 2 with P_{S_2} = 10^{-6} and P_{O_2} = 10^{-20} atm at 800°C. (*a*) 5 min. (*b*) 10 min.

M25402

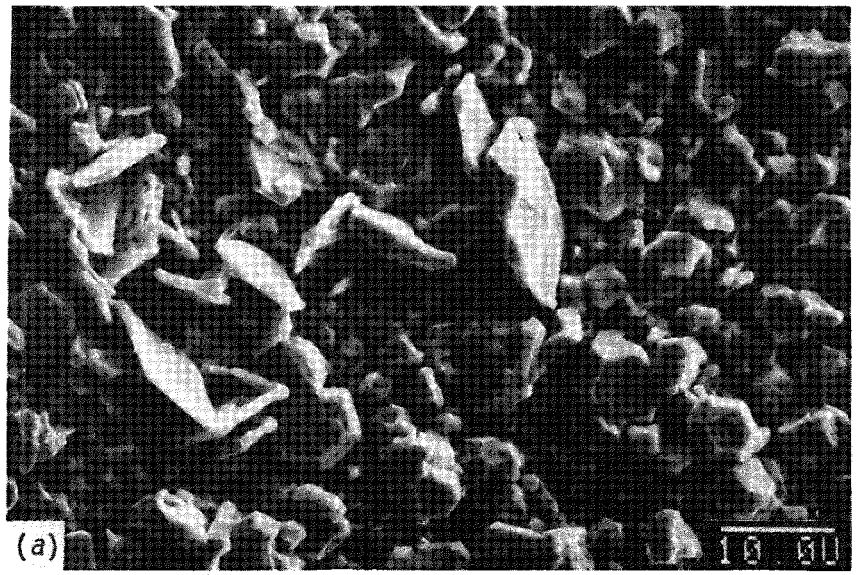

M25403

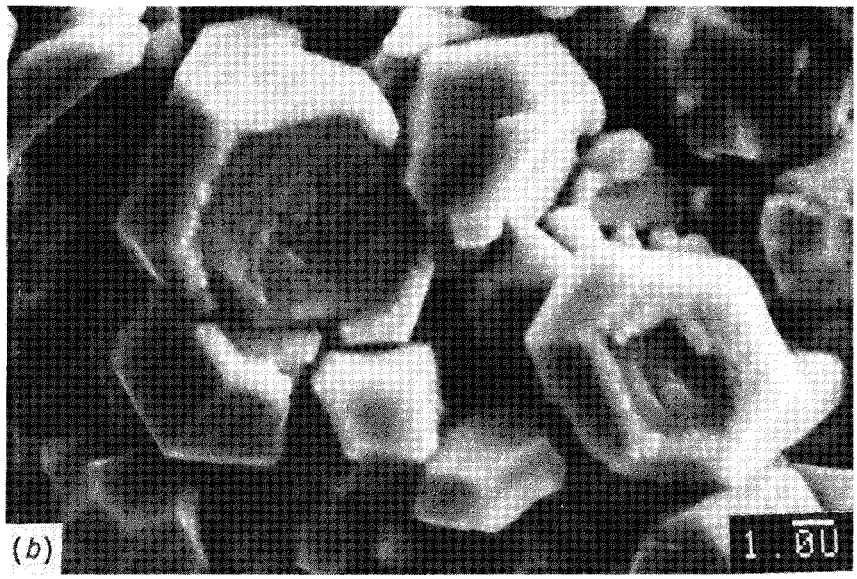

Fig. 4. (*a*) Surface topographies of PS2 (Fe-18Cr-6Al) exposed to gas mixture 2 with $P_{S_2} = 10^{-6}$ and $P_{O_2} = 10^{-20}$ atm at 800°C for 30 min. (*b*) A higher magnification of (*a*).

chromium-rich sulfide. Therefore, after a longer period of exposure of PS2 to the mixed gas, the iron-rich sulfide becomes the major corrosion product in the scale. Figures 5(*a*) and (*b*) show the topography and the cross section of the scale, respectively, after a 24-h exposure of PS2 to the same mixed gas. The iron-rich sulfide, $(Fe_{0.73}Cr_{0.24}Al_{0.03})S$, continued growing to produce a thick, porous layer on PS2. Only a relatively thin layer of sulfide enriched with chromium and aluminum was detected between the iron-rich sulfide scale and the metal substrate. In addition, some internal sulfidation can also be observed in Fig. 5(*b*).

Figure 6 shows the scale cross section on alloy PS3 (9% Cr, 9% Nb) after exposure to gas mixture 2 at 800°C for 24 h. It formed an outer iron-rich sulfide $(Fe_{0.8}Cr_{0.2})S$ layer and an inner porous sulfide layer. The formation of the inner porous layer is caused by internal sulfidation, which is actually more severe for PS3 than for PS2. The corrosion rate of PS4 (18% Nb) is a factor of ~5 slower than that of PS2 and proceeds by the formation of iron sulfide particles on a thin oxide layer, as shown in Fig. 7. The growth of these iron sulfide particles is responsible for most of the corrosion on PS4. Negligible internal sulfidation was observed. Also, the growth of the iron sulfide particles shows no obvious correlation with the appearance of second-phase precipitates in PS3 and PS4.

Reducing the H_2S concentration while increasing the activity of oxygen (keeping the sulfur activity constant) changed both the weight change and topography of the sulfide formed on PS4. Figure 8 compares thermogravimetric analysis (TGA) data for alloys exposed at 800°C to gas mixtures 1 ($P_{O_2} = 10^{-17.9}$ atm, H_2S = 0.0556%) and 2 ($P_{O_2} = 10^{-20}$ atm, H_2S = 0.56%), respectively. The surface topography and cross section of the scale formed in mixture 1 after 92 h (shown in Fig. 9) contrast with the scale formed in mixture 2 (shown in Fig. 7). Sulfide nodules in Fig. 9 have obviously grown out of the second-phase particles open to the surface, whereas the matrix phase is free of nodules and is covered by a thin continuous scale, identified by X-ray analysis as Al_2O_3. There is also evidence of internal sulfidation (identified as niobium sulfides) in the near-surface region of the second-phase particles (Fig. 9).

M24923

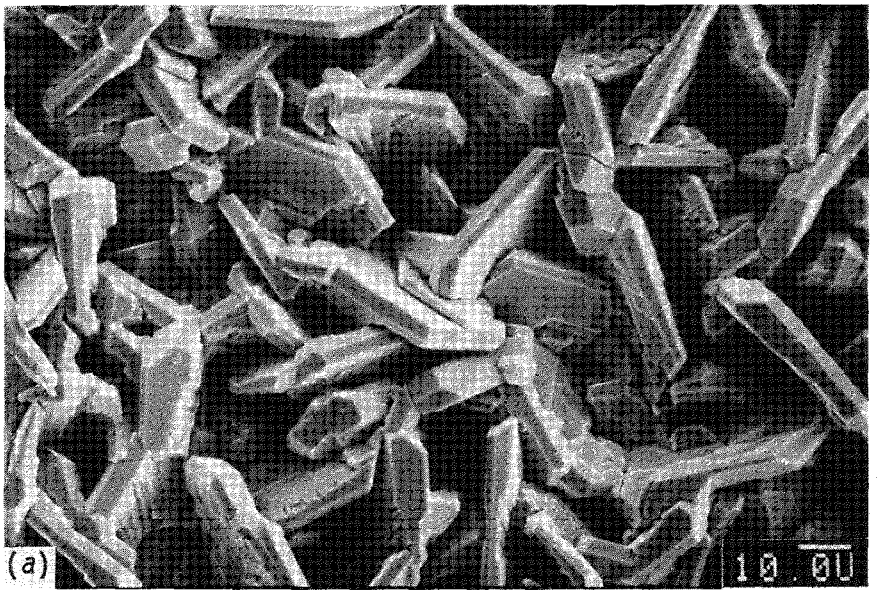

M24979

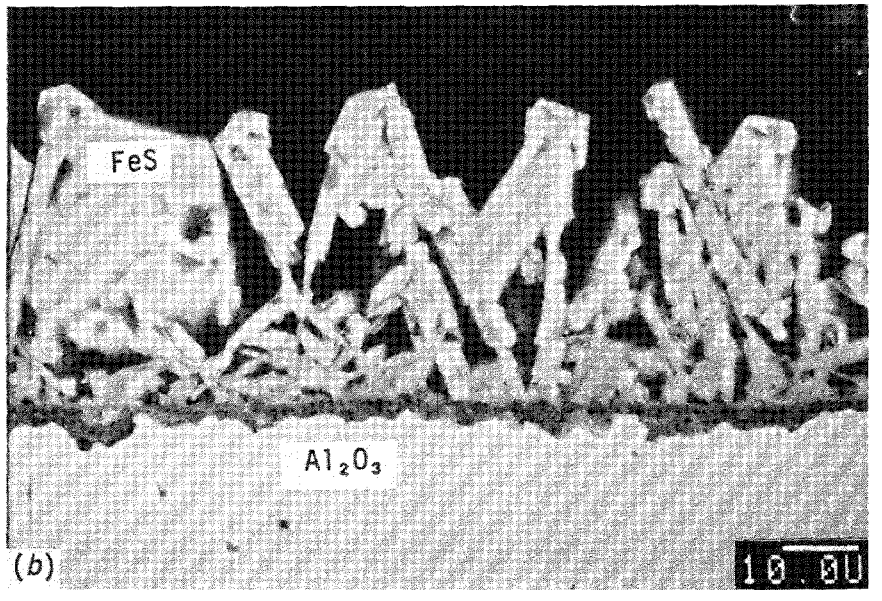

Fig. 5. (*a*) Topography of the scale and (*b*) cross section of the scale formed on PS2 (Fe-18Cr-6Al) exposed to gas mixture 2 with $P_{S_2} = 10^{-6}$ and $P_{O_2} = 10^{-20}$ atm at 800°C for 24 h.

M25718

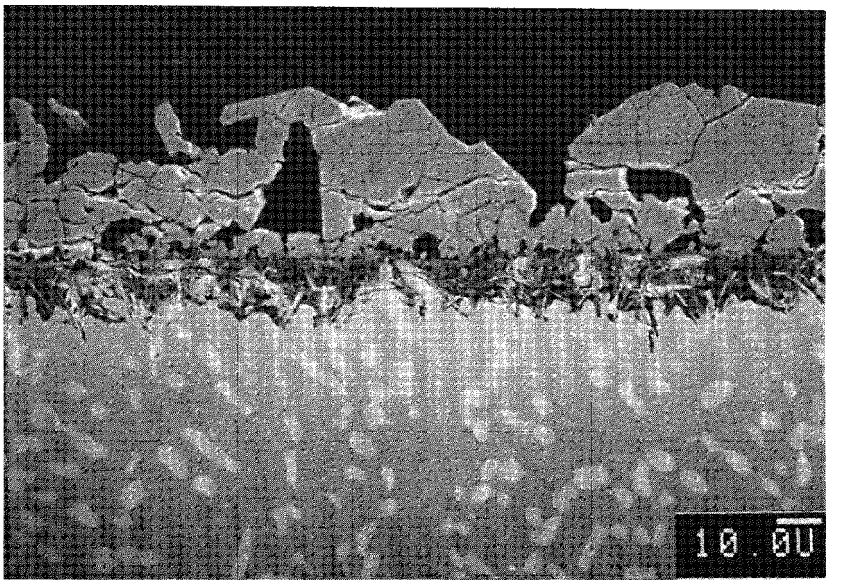

Fig. 6. Cross section of PS3 (Fe-9Cr-9Nb-6Al) after exposure to gas mixture 2 with P_{S_2} = 10^{-6} and P_{O_2} = 10^{-20} atm at 800°C for 24 h. Particles on the surface of sample are metal sulfides.

M25717

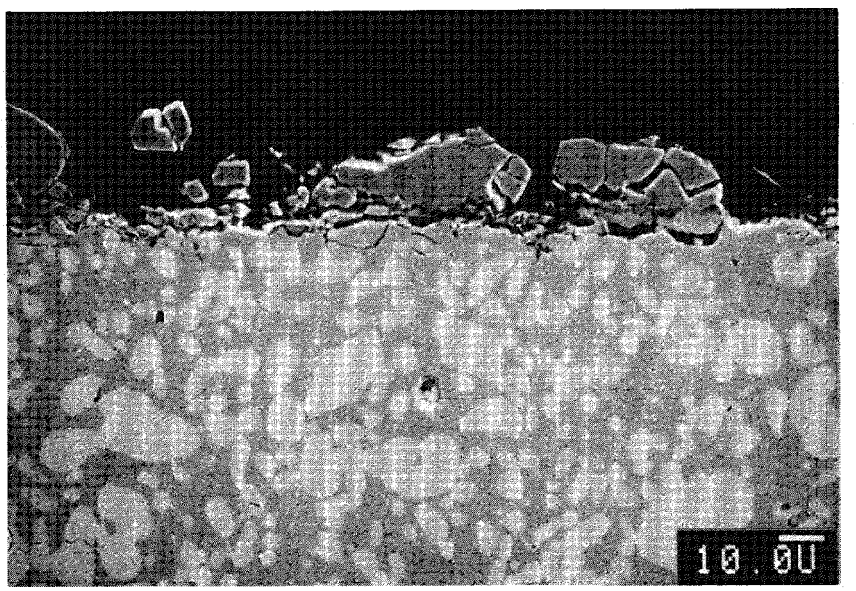

Fig. 7. Cross section of PS4 (Fe-18Nb-6Al) after exposure to gas mixture 2 with P_{S_2} = 10^{-6} and P_{O_2} = 10^{-20} atm at 800°C for 74 h.

ORNL-DWG 89-2178

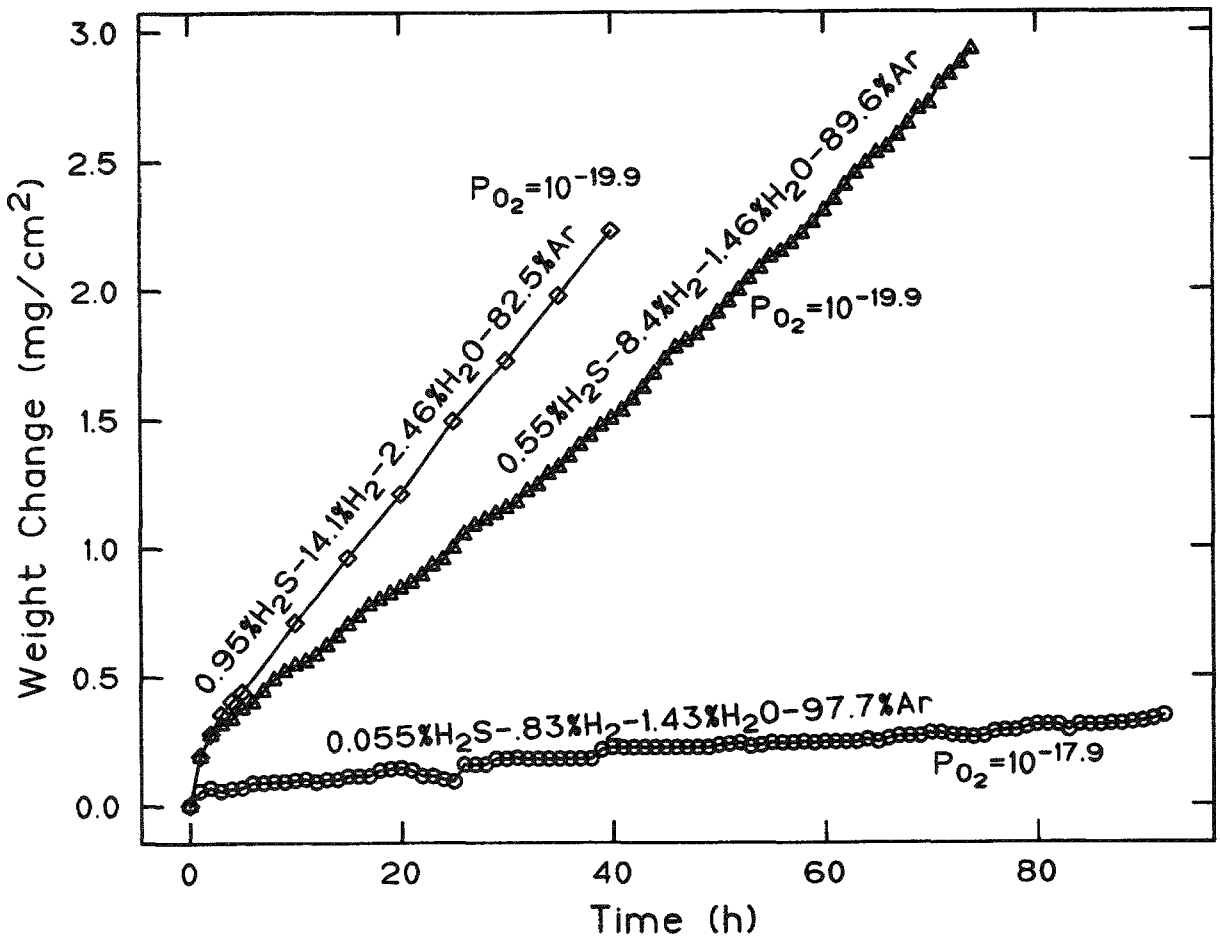

Fig. 8. TGA data for PS4 (Fe-18Nb-6Al) in gas mixtures 1 (P_{S_2} = 10^{-6} atm, P_{O_2} = 10^{-18} atm) and 2 (P_{S_2} = 10^{-6} atm, P_{O_2} = 10^{-20} atm) at 800°C.

To better define the respective roles of niobium and aluminum in the corrosion processes, the aluminum content of alloys PS8 (hot swaged) and PS10 (hot extruded) was increased to 12% (compared to 6% in PS4), keeping niobium constant at 18%. This increase in aluminum lowered the 100-h weight gain in H_2S-H_2-H_2O at 800°C by more than an order of magnitude compared with PS4. Furthermore, reducing the oxygen activity from 10^{-20} to 10^{-22} while increasing the H_2S level from 0.95 to 5.35 vol % had little effect on the weight gain of the 12% Al alloys (Fig. 10). Although the average size of second-phase particulates was slightly smaller for the

M25506

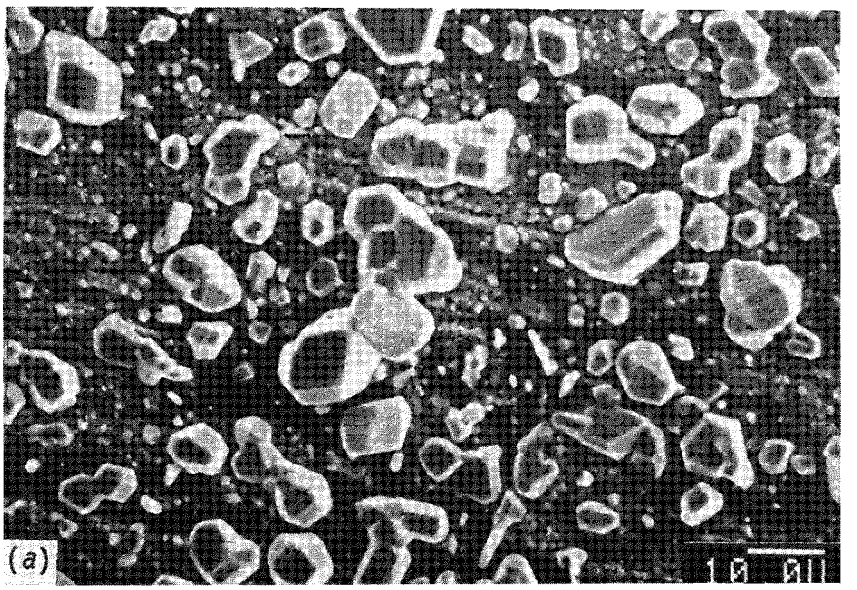

M25607

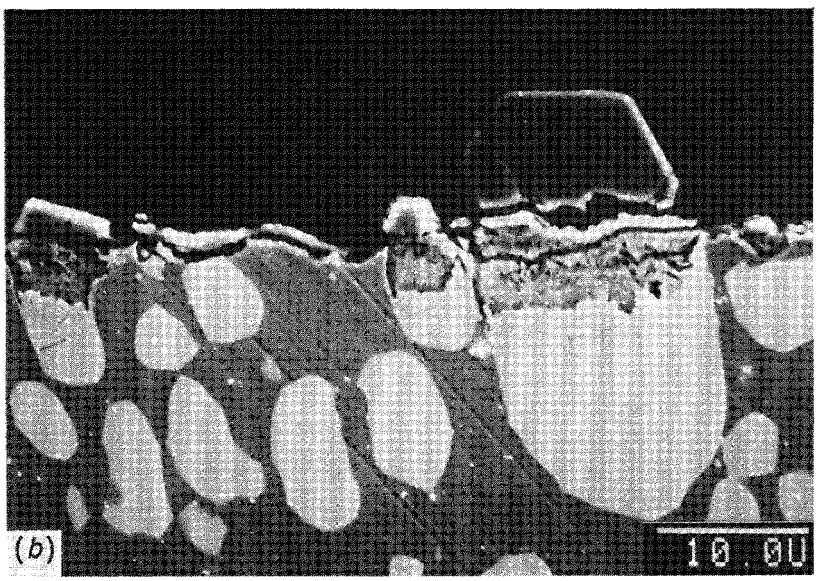

Fig. 9. Topography (*a*) and cross section (*b*) of the scale from corrosion of PS4 in gas mixture 1 with $P_{S_2} = 10^{-6}$ and $P_{O_2} = 10^{-18}$ atm at 800°C after 92 h.

ORNL-DWG 89-2179

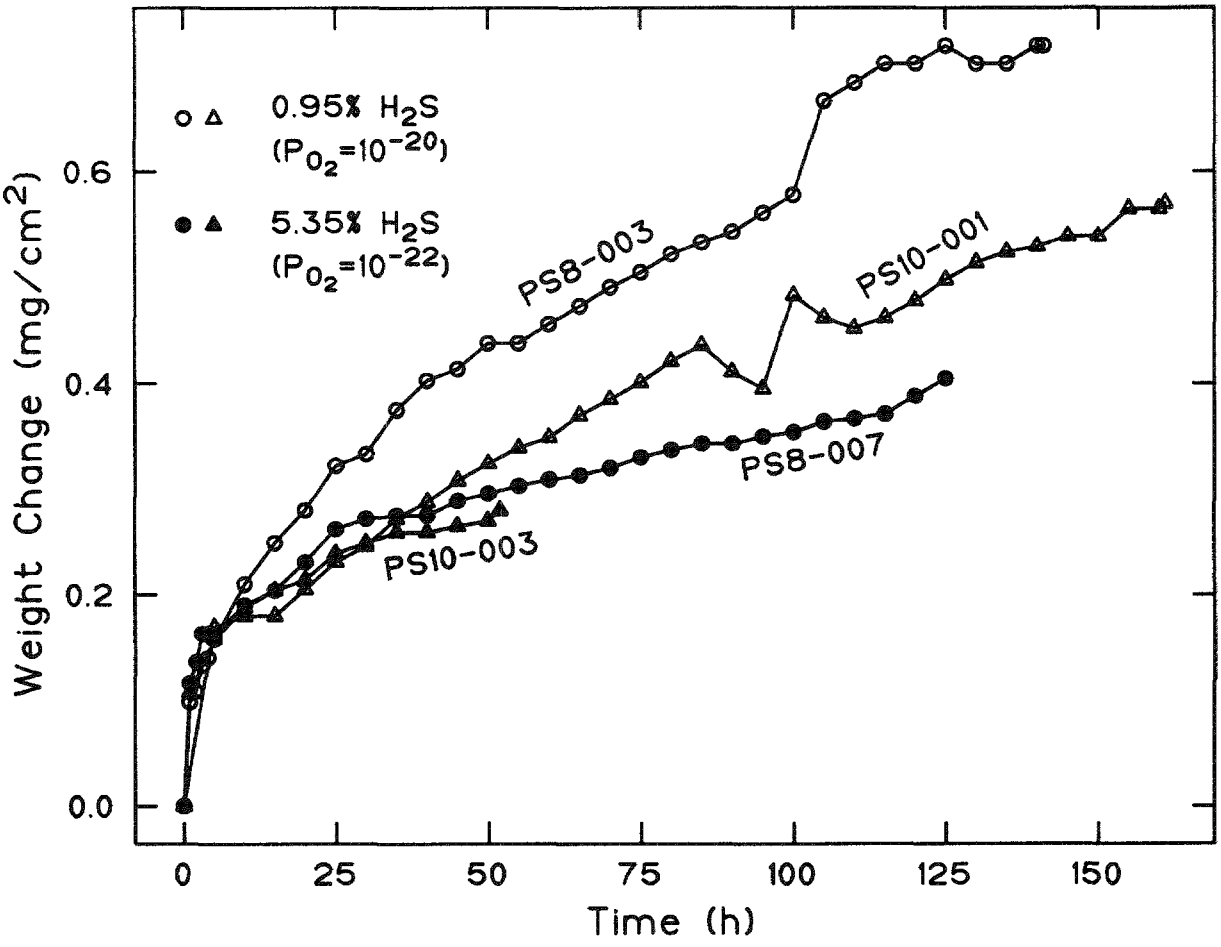

Fig. 10. Effect of H_2S pressure on weight change of Fe-18Nb-12Al at 800°C.

extruded alloy (PS10), there was no consistent difference in the weight change or scale morphology for this alloy compared with the hot-swaged alloy. Scanning electron microscopy (SEM) examinations showed the alloy surfaces to be covered uniformly by an extremely thin Al_2O_3 scale. However, a number of iron sulfide crystals projected outward from the scale-gas interface, appearing as thin, highly faceted blades [Fig. 11(*a*)]. Niobium sulfides were detected at the scale-metal interface and were epitaxial with the higher niobium-containing alloy phase present in the two-phase microstructure, as pictured in Fig. 11(*b*). Internal

M26924

M25607

Fig. 11. Topography (*a*) and cross section (*b*) of the Fe-18Nb-12Al alloy (PS8) after exposure for 125 h at 800°C in 79% H_2-5.4% H_2S-1.6% Al_2O-Ar (mixture 4).

sulfidation of the second-phase particles was similar to that for the 6% Al alloy [compare Fig. 9(*b*) with Fig. 11(*b*)].

Concurrently with the testing of the Fe-Nb-Al alloys, corrosion tests were initiated with Fe-Al alloys, whose properties are described in ref. 6. A binary Fe-Al alloy containing 15.8% Al (PS11) afforded a reasonably close match in aluminum concentration to the Fe-18Nb-12Al alloy (PS8 and 10). The former alloy is single phase (entirely within the Fe_3Al phase field), whereas the latter alloy is composed of a matrix phase containing 1.5% Nb, 13% Al, bal Fe, and a coarsely dispersed second phase containing 42.7% Nb, 7% Al, bal Fe. Two of the curves in Fig. 12 depict

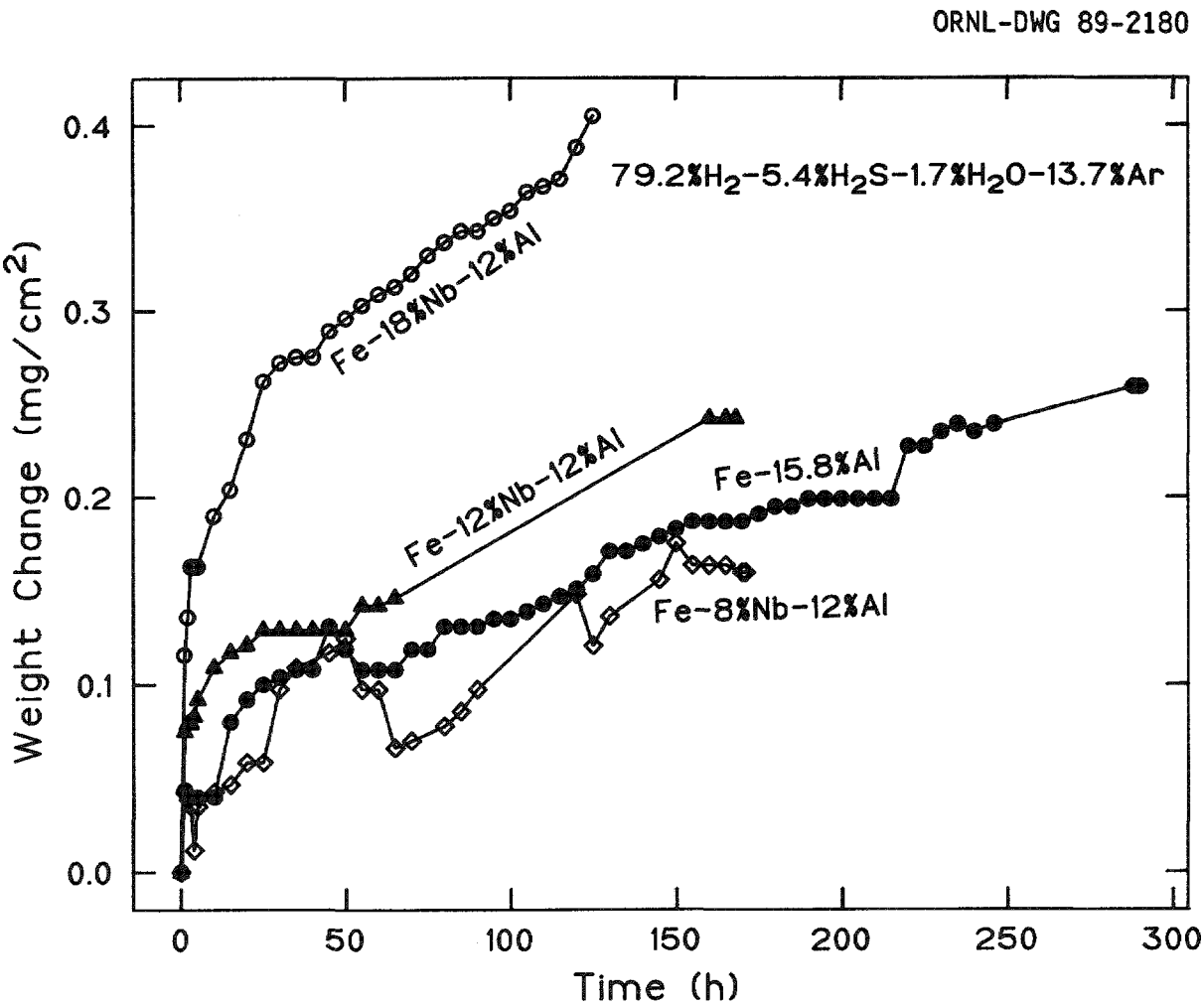

Fig. 12. Effect of decreasing niobium content on weight changes of Fe-Nb-Al alloys at 800°C.

the weight changes for the respective alloys recorded at 800°C in gas mixture 4 (5.35% H_2S, $P_{O_2} = 10^{-22}$ atm) and show that the weight gain of the binary alloy was less than that of the 18% Nb alloy. Subsequent microscopic analysis indicated that the corrosion product scale formed on the binary alloy consisted entirely of Al_2O_3, with no evidence of sulfides at either the scale-gas or scale-metal interfaces. As shown in Fig. 13, the scales on the PS11 and underlying substrate were quite featureless although significant spalling of the scale was apparent after the test.

The excellent performance of the binary Fe-Al alloy at the 15.8% Al level is indicative that aluminum content may be a much more significant factor than the niobium content in establishing the corrosion performance of the Fe-18Nb-12Al alloy (PS8 and 10). Accordingly, two additional Fe-Nb-Al alloys containing 12% Al but with lowered niobium contents (12 and 8%, respectively) were tested in the 5.35% H_2S mixture (Table 2) at 800°C. The microstructures of the 12 and 8% Nb alloys were composed of a matrix phase low in niobium and a secondary phase relatively high in niobium, very similar in composition to the second phase in the 18% Nb

YP6452

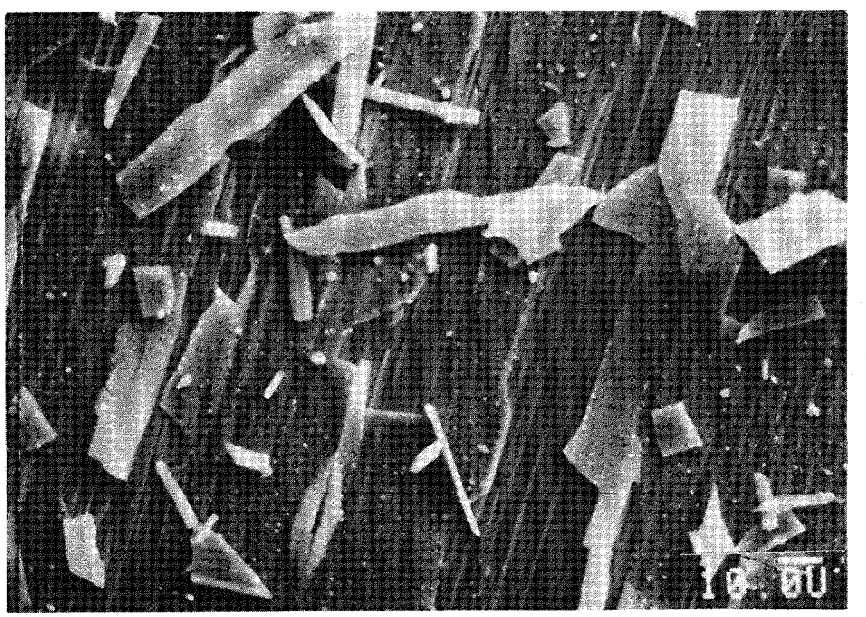

Fig. 13. Spalling of extremely thin oxide films formed at 800°C and then cooled.

alloys. The major difference was in the volume of the second phase, which decreased in proportion to the reduction in niobium content. Weight gains for the niobium-containing alloys are also compared with those for the 15.8% Al alloy in Fig. 12. Note that the alloys containing <18% Nb were comparable in performance to the binary Fe-Al alloy. Examination of the corrosion product scales showed discrete iron sulfide crystals growing outward from the oxide-covered surface, similar to those found on the 18% Nb alloy (Fig. 11). However, fewer of these crystals formed as the niobium content decreased, and only a few isolated crystals were found on the 8% Nb alloy.

DISCUSSION

Of the classes of alloys investigated, two stand out as highly resistant to H_2S-H_2-H_2O mixtures with relatively low oxygen partial pressures. They are, respectively, binary Fe-Al alloys containing ~16 wt % Al and Fe-Al-Nb alloys containing a minimum of 12 wt % Al and no chromium. The results also show that adding chromium to alloys containing 6 wt % Al is very detrimental to corrosion in the same type of gas mixture. The following discussion considers the interactive effects of Cr, Nb, and Al on the sulfidation/oxidation response of the alloys studied.

CHROMIUM

The so-called FeCrAl class of alloys, of which PS2 (Fe-18Cr-6Al) is representative, are extremely resistant to oxidation by air and steam environments at temperatures well above those set by mechanical property limits (~1000°C). Although the alloys rely mainly on the formation of alumina for corrosion protection, chromium plays an essential role in "stabilizing" the alumina scale. As shown by the phase-stability diagram in Fig. 14, the oxides of aluminum and chromium at ~700°C should both be favored thermodynamically in the H_2S-H_2-H_2O environments used in this study; however, the partial pressure of oxygen used in these tests is within 2 to 4 orders of that which defines the phase boundary between

ORNL-DWG 88-13388

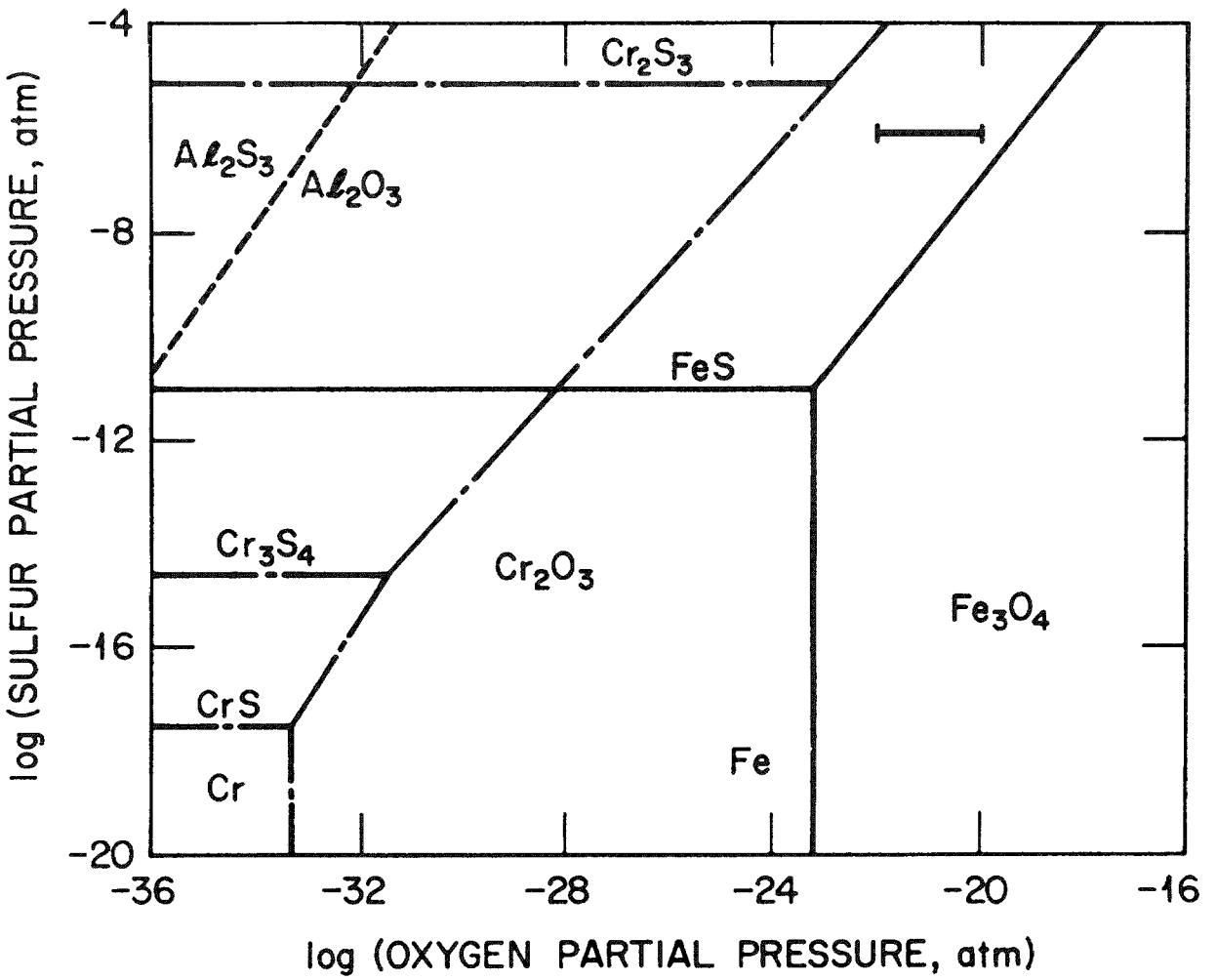

Fig. 14. Thermochemical M-S-O stability diagram at 650°C. (Test conditions denoted by bar.)

Cr_2O_3 and Cr_3S_4 at 700°C. Natesan[7] has shown that, under such a condition, the formation of chromium sulfide tends to be kinetically favored over chromium oxide. Furthermore, at 800°C, the phase boundary for Cr_2O_3/Cr_3S_4 shifts to still higher P_{O_2}, so that Cr_3S_4 is favored thermodynamically at this temperature under our gas conditions. These observations are consistent with the reaction products formed during exposure at 700 to 800°C, which included a continuous Al_2O_3 layer and nodules of chromium and iron sulfides (Fig. 5). Thus, unlike in air, in our relatively reducing H_2S-H_2-H_2O environment, chromium plays a detrimental rather than

beneficial role in alumina formation. This detrimental effect relates to competing reactions to form chromium and iron sulfides, whose growth rates are several orders of magnitude greater than that of Al_2O_3 at the temperatures of interest. Even when the Fe-18Cr-6Al alloy was preoxidized in air or in CO/CO_2 mixtures,[2] the protection of the preformed alumina film was eventually degraded by the formation of chromium sulfide. Likewise, adding even as little as 3 to 4% Cr to the binary Fe-15.8Al alloy (PS11) resulted in a significant increase in weight change attributable to sulfide formation in H_2S-H_2-H_2O under the present test conditions.[8]

NIOBIUM

The effect of niobium on oxidation/sulfidation is less clear than the effect of chromium. The replacement of chromium with niobium in alloys containing 6% Al resulted in a dramatic improvement in corrosion resistance to H_2S-H_2-H_2O mixtures. However, the improvement appears to derive more from the removal of chromium than from any direct beneficial effect of niobium. This conclusion is supported by (1) the further improvement in sulfidation/oxidation resistance as aluminum was increased from 6 to 12% while holding niobium at the 18% level, (2) the superior corrosion resistance of the Fe-15.8Al alloy containing no niobium, and (3) an actual decrease in weight gain at the 12% Al level as the niobium content was reduced to 12 and 8%, respectively. However, niobium may exert an indirect effect that is beneficial in these alloys by virtue of its effect on the aluminum distribution in the alloy microstructure. In contrast to the single-phase Fe-18Cr-6Al and Fe-15.8Al alloys, the microstructure of the reference Fe-Nb-Al alloys (≥8% Nb) is made up of two phases of unlike composition. The matrix phase contains relatively little niobium (≤2 wt %), whereas the discrete particles making up the second phase are relatively rich in niobium (>33 wt %) and contain less than 7 wt % Al. Thus, adding niobium effectively increases the aluminum content of the matrix phase compared with the nominal aluminum concentration in the alloy. Considering the improvement in corrosion resistance observed in alloys containing ≥12 wt % Al compared with 6% Al, this partitioning of aluminum to the matrix phase may be of some benefit to the

overall corrosion performance of the 6% Al alloy. However, the niobium content also determines the relative volume of the niobium-rich second phase in the alloy, and in this context, increasing the niobium content appears to have a negative effect. Even though the respective chemical compositions of the matrix and particulate phases were similar in the alloys containing 8, 12, and 18% Nb, the corrosion rate, based on weight change, increased as the niobium content and relative volume of the second phase increased (Fig. 12). This observation is consistent with the metallographic observation that the principal mode of attack of these alloys was by sulfidation of the exposed second-phase particulates (Fig. 11).

The hoped-for effect in these alloys was the growth of a protective niobium sulfide in association with aluminum oxide and improved adherence and/or mechanical properties of the alumina. Although both aluminum- and niobium-containing products were found in association with the niobium-rich second phase, the extent of sulfidation of this phase was greater than reported in experiments with pure niobium.[3,4] Obviously, the presence of an additional sulfide former, such as iron, interferes with the growth of a coherent and protective niobium sulfide layer. The aluminum concentration of the discrete phase (essentially Fe_2Nb) in the Fe-Nb-12Al alloys is ~6%. As discussed later, solid-solution alloys containing 12 to 16% Al (i.e., Fe_3Al-type alloys) are markedly superior in sulfidation resistance to alloys with 6% Al. Thus, it is of interest to consider the effect of relatively large niobium concentrations (≥20%) in a solid-solution matrix with 12% aluminum. (This test would require some form of nonequilibrium processing, such as rapid solidification or ion implantation.) In such a material, the niobium might play the desired role of a selective, refractory sulfide former, given the ability of the oxide scale to limit the nucleation of iron sulfide.

ALUMINUM

The alloying effects associated with aluminum are of particular importance to future alloy development. As discussed above, increasing the aluminum level from 6 to 12% significantly improved the sulfidation

resistance of the niobium-containing alloys, an improvement that was manifested by the matrix phase of the alloys. At the 6% Al level (without chromium), the matrix phase was relatively resistant to sulfidation at the higher oxygen activity (Fig. 6) but was subject to sulfidation of iron at the lower oxygen activity (Fig. 7). At the 12% Al level, this matrix phase was similar in sulfidation resistance to the binary Fe-15.8Al alloy (PS11) and was unaffected even by the higher H_2S pressures (Fig. 10). The solubility limit of niobium in the matrix phase at 12% Al is <2%, and at that level it appears to have no effect on sulfidation resistance.

The mechanism by which aluminum completely suppresses sulfidation of iron in the Fe-Nb-12Al matrix phase and Fe-15.8Al alloys is now under study. As is obvious from Figs. 11 and 12, the Al_2O_3 scale that forms on these alloys, while extremely thin, is subject to spalling when it cools to room temperature. Nevertheless, thermal cycling these alloys in H_2S-H_2-H_2O gas mixtures from 800°C to room temperature every 48 h had only a minor effect on weight change over a 168-h interval.[8] Furthermore, there was no evidence of sulfide formation on the thermally cycled specimen following exposure. Adding chromium to the Fe-15.8Al alloy, even in amounts as low as 4%, led to the relatively rapid growth of chromium and iron-sulfide nodules above the scale and even to the formation of Al_2S_3 within the scale.[8] However, preoxidation of an Fe-15.8Al-5Cr alloy in air effectively suppresses sulfidation for periods as long as 200 h at 800°C (in isothermal tests). These observations confirm that the growth rate of the Al_2O_3 scale is extremely fast compared with formation of iron sulfide at the 12 to 15.8% Al level. They also indicate that, under sulfidizing conditions, chromium acts to prevent the growth of a protective Al_2O_3 layer rather than to disrupt an initially protective oxide layer.

CONCLUSIONS

1. In H_2S-H_2-H_2O gas mixtures that are relevant to coal gasification, the sulfidation/oxidation resistance of Fe-18Cr-6Al alloys can be improved significantly through alloying with niobium in place of chromium.

2. Substituting niobium for chromium at the 6% Al level reduced the 100-h weight gain at 800°C by a factor of at least 5. However, significant amounts of FeS were found at the scale-gas interface, together with some sulfidation of niobium at the metal-scale interface.

3. Substituting niobium for chromium and increasing aluminum to 12 wt % dramatically reduced the corrosion rate in H_2S-H_2-H_2O. There was no evidence of sulfidation of the matrix phase in these alloys, but second-phase particles similar in composition to Fe_2Nb underwent internal sulfidation.

4. Reducing the niobium level from 18 to 12 or 8%, respectively, actually reduced the weight gain (sulfidation) at 800°C. The reduction was the result of a lower volume fraction of the Fe_2Nb phase in the latter alloys. Thus, for Fe-Nb-12Al alloys, aluminum appears to be a more significant factor in inhibiting sulfidation than is niobium.

5. Achieving a protective niobium sulfide reaction product in association with an aluminum oxide scale might be possible in a nonequilibrium alloy matrix containing a niobium concentration at least equal to the aluminum concentration. Such an alloy would require processing by rapid solidification or ion implantation.

6. A major finding in these studies was the complete suppression of iron sulfide formation in the matrix phase of the Fe-Nb-12Al alloys and the binary Fe_3Al alloy containing 15.8 wt % Al. The Fe_3Al alloy showed a negligible weight gain even after 300-h exposure to H_2S-H_2-H_2O at 800°C. Although the alumina scale formed on Fe_3Al is subject to spalling on cooling to room temperature, the corrosion rate of the alloy was not significantly affected by thermal cycling to room temperature at 50-h intervals during a 168-h exposure at 800°C. Furthermore, there was no evidence of sulfide formation on the thermally cycled specimen following exposure.

REFERENCES

1. H. S. Hsu, *A Review of the Development and Breakdown of Protective Oxide Scales Exposed to Coal-Derived Atmospheres*, ORNL-6323, 1986.

2. H. S. Hsu, "Corrosion-Resistant Scales on Iron Based Alloys," pp. 321–42 in *Fossil Energy Materials Program Conference Proceedings*, ORNL/FMP-87/4, 1987.

3. C. G. McKamey et al., *Development of Iron Aluminides for Coal Conversion Systems*, ORNL/TM-10793, July 1988.

4. S. Mrowec and K. Przybylski, "Transport Properties of Sulfide Scales and Sulfidation of Metals and Alloys," *J. Oxid. Met.* 23, 107 (1985).

5. K. N. Strafford and J. R. Bird, "The Kinetics of Sulphidation of Niobium," *J. Less-Common Met.* 68, 223 (1979).

6. K. Natesan, "High Temperature Corrosion in Coal Gasification Systems," *Corrosion* 41, 646 (1985).

7. K. Natesan, "High Temperature Alloy Corrosion in Coal Conversion Environments," pp. 336-44 in *High Temperature Corrosion*, NACE-6, National Association of Corrosion Engineers, 1983.

8. J. H. DeVan, "Oxidation Behavior of Fe_3Al and Derivative Alloys," *Oxidation of High Temperature Intermetallics*, The Metallurgical Society of AIME (in press).

ORNL/TM-11176

INTERNAL DISTRIBUTION

1–2. Central Research Library
3. Document Reference Section
4–5. Laboratory Records Department
6. Laboratory Records, ORNL RC
7. ORNL Patent Section
8–10. M&C Records Office
11. P. Angelini
12. R. L. Beatty
13. T. M. Besmann
14. P. J. Blau
15. D. N. Braski
16. P. T. Carlson
17. O. B. Cavin
18. D. F. Craig
19–23. J. H. DeVan
24. J. R. DiStefano
25. J. I. Federer
26. R. S. Holcomb
27. J. A. Horton, Jr.
29–32. M. Howell
33–37. H. S. Hsu
38. C. R. Hubbard
39. R. R. Judkins
40. J. R. Keiser
41. O. F. Kimball
42. C. T. Liu
43. J. R. Mayotte
44. P. J. Maziasz
45. H. E. McCoy, Jr.
46. C. G. McKamey
47. R. E. Pawel
48. P. L. Rittenhouse
49. A. C. Schaffhauser
50. V. K. Sikka
51. J. L. Scott
52. G. M. Slaughter
53. J. O. Stiegler
54. R. W. Swindeman
55. P. F. Tortorelli
56. J. R. Weir, Jr.
57. D. F. Wilson
58. A. D. Brailsford (Consultant)
59. H. D. Brody (Consultant)
60. F. F. Lange (Consultant)
61. D. P. Pope (Consultant)
62. E. R. Thompson (Consultant)
63. J. B. Wachtman, Jr. (Consultant)

EXTERNAL DISTRIBUTION

64–65. AIR PRODUCTS AND CHEMICALS, P.O. Box 538, Allentown, PA 18105

S. W. Dean
S. C. Weiner

66. ALBERTA RESEARCH COUNCIL, Oil Sands Research Department, P.O. Box 8330, Postal Station F, Edmonton, Alberta, CANADA T6H5X2

L. G. S. Gray

67. ARGONNE NATIONAL LABORATORY, 9700 South Cass Avenue, Argonne, IL 60439

K. Natesan

68. ARGONNE NATIONAL LABORATORY-WEST, P.O. Box 2528, Idaho Falls, ID 83403-2528

S. P. Henslee

69. AVCO RESEARCH LABORATORY, 2385 Revere Beach Parkway, Everett, MA 02149

R. J. Pollina

70–71. BABCOCK & WILCOX, 1562 Beeson Street, Alliance, OH 44601

T. I. Johnson
T. Modrak

72. BABCOCK & WILCOX, Domestic Fossil Operations, 20 South Van Buren Avenue, Barberton, OH 44023

M. Gold

73. BABCOCK & WILCOX, Lynchburg Research Center, P.O. Box 11165, Lynchburg, VA 24506

H. Moeller

74–75. BATTELLE-COLUMBUS LABORATORIES, 505 King Avenue, Columbus, OH 43201

V. K. Sethi
I. G. Wright

76. BRITISH GAS CORPORATION, Westfield Development Centre, Cardenden, Fife, SCOTLAND KY5OHP

J. E. Scott

77. BROOKHAVEN NATIONAL LABORATORY, Department of Applied Science, Upton, Long Island, NY 11973

T. E. O'Hare

78–79. CANADA CENTER FOR MINERAL & ENERGY TECHNOLOGY, 568 Booth Street, Ottawa, Ontario, CANADA K1AOG1

R. Winston Revie
Mahi Sahoo

80. CASE WESTERN RESERVE UNIVERSITY, Department of Metallurgy & Materials Science, 516 White Building, 10900 Euclid Avenue, Cleveland, OH 44106

K. M. Vedula

81. COMBUSTION ENGINEERING, INC., 911 West Main Street, Chattanooga, TN 37402

D. A. Canonico

82. CONSOLIDATION COAL COMPANY, 4000 Brownsville Road, Library, PA 15129

S. Harding

83. EBASCO SERVICES, INC., P.O. Box 1002, Glen Rose, TX 76043

T. A. Flynn

84–87. ELECTRIC POWER RESEARCH INSTITUTE, P.O. Box 10412, 3412 Hillview Avenue, Palo Alto, CA 94303

W. T. Bakker
R. L. S. Chang
J. T. Stringer
R. H. Wolk

88. EUROPEAN COMMUNITIES JOINT RESEARCH CENTRE, Petten Establishment, P.O. Box 2, 1755 ZG Petten, THE NETHERLANDS

M. Van de Voorde

89. FOSTER WHEELER DEVELOPMENT CORPORATION, Materials Technology Department, John Blizard Research Center, 12 Peach Tree Hill Road, Livingston, NJ 07039

J. L. Blough

90. GAS RESEARCH INSTITUTE, 8600 West Bryn Mawr Avenue, Chicago, IL 60631

H. S. Meyer

91. GENERAL ELECTRIC COMPANY, One River Road, Building 55, Room 115, Schenectady, NY 12345

R. W. Haskell

92. LAWRENCE BERKELEY LABORATORY, University of California, Berkeley, CA 94720

A. V. Levy

93. LAWRENCE LIVERMORE LABORATORY, P.O. Box 808, L-325, Livermore, CA 94550

W. A. Steele

94. MASSACHUSETTS INSTITUTE OF TECHNOLOGY, Department of Civil Engineering, 77 Massachusetts Avenue, Room I-280, Cambridge, MA 02139

O. Buyukozturk

95. MOBIL RESEARCH & DEVELOPMENT CORPORATION, P.O. Box 1026, Princeton, NJ 08540

R. C. Searles

96–97. NATIONAL INSTITUTE OF STANDARDS AND TECHNOLOGY, Materials Building, Gaithersburg, MD 20899

S. J. Dapkunas
H. M. Ondik

98. NATIONAL MATERIALS ADVISORY BOARD, National Research Council, 2101 Constitution Avenue, Washington, DC 20418

K. M. Zwilsky

99. NEW ENERGY DEVELOPMENT ORGANIZATION, Sunshine 60 Building, P.O. Box 1151, 1-1, Higashi-Ikebukuro 3-chrome, Toshima-Ku, Tokyo, 170, JAPAN

S. Ueda

100. OAK RIDGE ASSOCIATED UNIVERSITIES, P.O. Box 117, Oak Ridge, TN 37831-0117

Beth Jinkerson

101. RISOE NATIONAL LABORATORY, P.O. Box 49, DK-4000, Roskilde, DENMARK

Aksel Olsen

102. SHELL DEVELOPMENT COMPANY, P.O. Box 1380, Houston, TX 77251-1380

L. W. R. Dicks

103. SOUTHERN CLEAN FUELS, P.O. Box 470, Wilsonville, AL 35186

A. J. Patko

104. SOUTHWEST RESEARCH INSTITUTE, 6620 Culebra Road, P.O. Drawer 28510, San Antonio, TX 78284

F. F. Lyle, Jr.

105. TENNESSEE VALLEY AUTHORITY, Energy Demonstration & Technology, MR 2N58A, Chattanooga, TN 37402-2801

C. M. Huang

106. TENNESSEE VALLEY AUTHORITY, 1101 Market Street, MR 3N57A, Chattanooga, TN 37402

R. Q. Vincent

107. TEXAS EASTERN TRANSMISSION CORPORATION, P.O. Box 2521, Houston, TX 77252

D. H. France

108. THE MATERIALS PROPERTIES COUNCIL, INC., United Engineering Center, 345 East Forty-Seventh Street, New York, NY 10017

M. Prager

109. THE TORRINGTON COMPANY, Advanced Technology Center, 59 Field Street, Torrington, CT 06790

W. J. Chmura

110. UNITED ENGINEERS & CONSTRUCTORS, 30 South 17th Street, P.O. Box 8223, Philadelphia, PA 19101

A. J. Karalis

111. UNIVERSAL ENERGY SYSTEMS, INC., 4401 Dayton-Xenia Road, Dayton, OH 45432

V. Srinivasan

112. UNIVERSITY OF CALIFORNIA AT BERKELEY, Department of Materials Science and Mineral Engineering, Berkeley, CA 94720

E. R. Parker

113. UNIVERSITY OF CALIFORNIA AT BERKELEY, Department of Mechanical Engineering, Berkeley, CA 94720

J.A.C. Humphrey

114. UNIVERSITY OF CALIFORNIA, LOS ANGELES, School of Engineering and Applied Science, Department of Materials Science, Los Angeles, CA 90024

D. L. Douglass

115. UNIVERSITY OF CINCINNATI, Department of Materials Science and Engineering, Cincinnati, OH 45221

R. Y. Lin

116–117. UNIVERSITY OF TENNESSEE AT KNOXVILLE, Department of Materials Science and Engineering, Knoxville, TN 37916

R. A. Buchanan
C. D. Lundin

118. UNIVERSITY OF TENNESSEE SPACE INSTITUTE, Tullahoma, TN 37388

Y.C.L. Wu

119. WESTINGHOUSE ELECTRIC CORPORATION, Research and Development Center, 1310 Beulah Road, Pittsburgh, PA 15235

S. C. Singhal

120. WESTINGHOUSE HANFORD COMPANY, P.O. Box 1970, W/A-65, Richland, WA 99352

R. N. Johnson

121–122. DOE, OAK RIDGE OPERATIONS OFFICE, P.O. Box 2001, Oak Ridge, TN 37831

Assistant Manager for Energy Research and Development
E. E. Hoffman

123. DOE, OFFICE OF BASIC ENERGY SCIENCES, Materials Sciences Division, ER-131, GTN, Washington, DC 20545

J. B. Darby

124. DOE, OFFICE OF CONSERVATION AND RENEWABLE ENERGY, Energy Conversion and Utilization Technologies Division, CE-12, Forrestal Building, Washington, DC 20545

J. J. Eberhardt

125–129. DOE, OFFICE OF FOSSIL ENERGY, Washington, DC 20545

D. J. Beecy (FE-14)
J. P. Carr (FE-14)
R. T. King (FE-14)
F. M. Glaser (FE-14)
T. B. Simpson (FE-25)

130–132. DOE, MORGANTOWN ENERGY TECHNOLOGY CENTER, P.O. Box 880, Morgantown, WV 26505

F. W. Crouse, Jr.
W. J. Huber
J. E. Notestein

133–135. DOE, PITTSBURGH ENERGY TECHNOLOGY CENTER, P.O. Box 10940, Pittsburgh, PA 15236

S. Akhtar
T. C. Rupel
J. W. Wiggins

136-145. DOE, OFFICE OF SCIENTIFIC AND TECHNICAL INFORMATION, Office of Information Services, P.O. Box 62, Oak Ridge, TN 37831

For distribution by microfiche as shown in DOE/TIC-4500, Distribution Categories UC-103 (Fluidized Bed Combustion), -109 [Coal Gasification (Surface and Underground)], and -114 (Coal Based Materials and Components).

☆U.S. GOVERNMENT PRINTING OFFICE 1989–648-119/00016